Mixing, Hypersalinity and Gradients in Hervey Bay, Australia

Ulf Gräwe · Jörg-Olaf Wolff · Joachim Ribbe

Received: date / Accepted: date

Abstract Hervey Bay, a large coastal embayment situated off the central eastern coast of Australia, is a shallow tidal area (average depth = 15 m), close to the continental shelf. It shows features of an inverse estuary, due to the high evaporation rate (approx. 2 m/year), low precipitation (less than 1 m/year) and on average almost no freshwater input from rivers that drain into the bay.

The hydro- and thermodynamical structure of Hervey Bay and their variability are presented here for the first time, using a combination of four-dimensional modelling and observations from field studies. The numerical studies are performed with the COupled Hydrodynamical Ecological model for REgioNal Shelf seas (COHERENS). Due to the high tidal range (> 3.5 m) the bay is considered as a vertically well-mixed system and therefore only horizontal fronts a likely. Recent field measurements, but also the numerical simulations indicate characteristic features of an inverse/hypersaline estuary with low salinities (35.5 psu) in the open ocean and peak values (> 39.0 psu) in the head water of the bay. The model further predicts a nearly persistent mean salinity gradient of 0.5 psu across the bay (with higher salinities close to the shore).

Ulf Gräwe, Jörg-Olaf Wolff
ICBM, Physical Oceanography (Theory), University of Oldenburg, Oldenburg, Germany
E-mail: graewe@icbm.de

Joachim Ribbe
Department of Biological and Physical Sciences, University of Southern Queensland, Toowoomba, Australia

The investigation further shows that air temperature, wind direction and tidal regime are mainly responsible for the stability of the inverse circulation and the strength of the salinity gradient across the bay.
Due to an ongoing drying trend, the occurrence of severe droughts at the central east coast of Australia and therefore a reduction in freshwater supply, the salinity flux out of the bay has increased and also the inverse circulation has strengthened.

Keywords Hypersalinity · inverse circulations · Hervey Bay, Australia · mixing

1 Introduction

In subtropical climates where evaporation is likely to exceed the supply of freshwater from precipitation and river run-off, large coastal bays, estuaries and near shore coastal environments are often characterised by inverse circulations and hypersalinity zones (Tomczak and Godfrey 2003, Wolanski 1986). An inverse circulation is characterised by sub-surface flow of saline water away from a zone of hypersalinity towards the open ocean. This flow takes place beneath a layer of inflowing oceanic water and leads to salt injections into the ocean (Brink and Shearman 2006). Secondly inverse circulations are characterised by a reversed density gradient.
The coastal zone in regular estuaries or bays is controlled by the riverine fresh water and therefore low densities. Inverse estuaries or bays on the other hand are characterised by high salinities in the coastal zone with inverse gradients for salinity and density directing offshore with minimal direct oceanic influence. Examples for such regions include the Gulf of California (Lavin et al. 1998), estuaries in Mediterranean-climate regions (Largier et al. 1997), Spencer Gulf (Lennon et al. 1987), the Ria of Pontevedra (deCastro et al. 2004) and the Gulf of Kachchh (Vethamony et al. 2007).
High evaporation during summer leads to an accumulation of salt in the head water of these inverse bays or estuaries. Following the season into autumn and winter these water masses are subsequently cooled and can become gravitationally unstable. Under certain circumstances they can evolve into gravity currents or plumes that flow out of the bay into the deeper ocean adjacent to the continental shelf. Due to strong tidal and wind induced mixing (either vertically or horizontally) these events should be of short duration. Efficient mixing homogenises the water column and instead of a two-layer structure in the vertical, one observes a more horizontally distributed frontal system

(Loder and Greenberg 1986).

The excess of evaporation over precipitation also induces a mass flux towards the shore. Due to the net loss of water (by evaporation) and to maintain the water balance, an inflow of water from the ocean is required and in the case of semi enclosed water bodies with restricted water exchange with the open ocean, this can have implications for the accumulation of salt, organic or inorganic tracers and pollutants.

In Australia, where climate is characterised by significant inter annual variability in rainfall (Murphy and Ribbe 2004), longer lasting trends in annual rainfall have been observed since about 1950 (Shi et al. 2008a). Along the east coast rainfall has declined by more than 200 mm (1951 - 2000). This reduction of about 20 % in total annual rainfall has caused persistent drought conditions in the last two decades. These shifts have been attributed to changes in large scale climate system processes such as the Southern Annular Mode, the Indian Ocean Dipole and the El Niño Southern Oscillation (Shi et al. 2008b). These changes, which are linked to a widening of the tropical belt, are projected to persist into the future. The adjustments are associated with an increased heat transport by the southward flowing East Australia Current (EAC) that has been attributed to atmospheric circulation changes (Cai et al. 2005). The changes in rainfall are accompanied by a rise in near surface atmospheric temperature that along the east coast of Australia is in the order of about 0.1 °C per decade (Beer et al. 2006).

In this paper a detailed description of the hydrodynamic and thermohaline structure of Hervey Bay is presented for the first time. Hervey Bay is a coastal embayment at the central East coast of Australia, which has attracted only little attention from the physical oceanography community during the last two decades. Middelton et al. (1994) lacked observational evidence in support of their hypothesis that Hervey Bay potentially exports high salinity water formed through a combination of heat loss, high evaporation and weak freshwater input in shallow regions of the bay. Ribbe (2006) showed that field observations suggest that Hervey Bay can be classified as an inverse bay and that indeed the excess of evaporation over precipitation leads to a salinity flux out of the bay.

This study explores in detail the mechanisms that lead to sub-surface flow of high saline waters out of the bay (gravity currents) and the stability of these flows. Recent hydrographical observations from Hervey Bay, Ribbe (2008b) (Fig. 1) and a coastal ocean general circulation model are used for this purpose.

The coastal bay is shown to be dominated by hypersalinity and an inverse circulation. Hypersalinity is a persistent feature and is more frequent in the last decade due to an ongoing drying trend and the occurrence of severe droughts.

2 The Region

Hervey Bay is a large coastal bay off the subtropical east coast of eastern Australia and is situated at the southern end of the Great Barrier Reef to the south of the geographic definition of the Tropic of Capricorn (23.5 °S). Fraser Island separates the bay to the east from the Pacific Ocean. At the northern tip of Fraser Island an enormous sandspit is located, to extend the separation from the open ocean further 30 kilometres north. This sandspit, called Breaksea Spit, has an average depth of 6 m and shows some dominant underwater dune features. Hervey Bay covers an area of about 4000 km^2. Mean depth is about 15 m, with depths increasing northward to more than 40 m, where the bay is connected to the open ocean via an approximately 60 km wide gap. A narrow and shallow ($<$ 2 m) channel (Great Sandy Strait) connects the bay to the ocean in the south. Two rivers connect the catchments area with the bay, the Burnett River at Bundaberg and the Mary River south of Urangan. In the East/Northeast of Fraser Island the continental shelf has an average width of 40 km. At the eastern shelf edge the East Australian Current (EAC) reattaches to the shelf to follow now the coastline to the south.

The climate around Hervey Bay is characterised as subtropical with no distinct dry period but with most precipitation occurring during the southern hemisphere summer. The region is influenced by the Trade winds from the east with a northern component in autumn and winter and a southern one in spring and summer (Tab. 1).

An interesting feature of Hervey Bay is that its length to width ratio is close to 1, whereas for example for Spencer Gulf, Gulf of California and Ria of Pontevedra this ratio is larger than 3. This has some implications on the water exchange in Hervey Bay and the maintenance of salinity/density gradients as will be shown below.

3 Model description

3.1 General features of COHERENS

We employ the hydrodynamic part of the three dimensional primitive equation ocean model COHERENS (COupled Hydrodynamical Ecological model for REgioNal Shelf seas) (Luyten et al. 1999). Some basic features of the model can be summarised as follows: the model is based on a bottom following vertical sigma coordinate system with spherical coordinates in the horizontal. The hydrostatic assumption and the Boussinesq approximation are included in the horizontal momentum equations. The sea surface can move freely, therefore barotropic shallow water motions such as surface gravity waves are included. The simulation of vertical mixing is achieved through the 2.5 order Mellor-Yamada turbulence closure (Mellor et al. 1982). The horizontal turbulence is taken proportional to the product of lateral grid spacing and the shear velocity (Smagorinsky 1963):

$$K_H = C_{Smag} \Delta x \Delta y \sqrt{(\partial_x u)^2 + (\partial_y v)^2 + 0.5\,(\partial_y u + \partial_x v)^2} \tag{1}$$

where C_{Smag} is a constant that should have a value between 0.1 ... 0.4 (0.25 in our case), $\Delta x, \Delta y$ is the grid spacing. Advection of momentum and scalar transport is implemented with the TVD (Total Variation Diminishing) scheme using the superbee limiting function (Roe 1985). These are standard configurations provided with COHERENS. For further details of numerical techniques employed see Luyten et al. (1999).

3.2 Boundary conditions

Because the simulations heavily rely on the proper calculations of air-sea fluxes, we modified the bulk parameterisations in COHERENS by the COARE 3.0 algorithm (Coupled-Ocean Atmosphere Response Experiment, Fairall et al. 1996, 2003). This algorithm now includes various physical processes, relating near-surface atmospheric and oceanographic variables and their relationship to the sea surface, to compute/estimate the transfer coefficients of latent heat, sensible heat, momentum and moisture. These transfer coefficients have a dependence on surface stability prescribed by the Monin-Obukov similarity theory (Monin 1953). Moreover the algorithm includes separate models for the ocean's cool skin and the diurnal warm layer, which are used to derive the true skin temperature. For details of the parameterisations and also the iterative solution techniques employed see Fairall et al. 1996, 2003.

The long wave back radiation flux is computed using the formulation of Bignami et al. (1995). This choice was motivated by the comparison of different back radiation parameterisations by Josey et al. (2003). Here the formulation of Bignami et al. (1995) showed the best performance in subtropical regions.

Amplitudes and phases of the five major tidal constituents (M_2, S_2, N_2, K_1 and O_1) are prescribed at the open boundary. These five principal constituents explain nearly 80% of the total variance of the observations within Hervey Bay. Tidal elevations and phases are taken from the output of the global tide model/atlas FES2004 (Lyard et al. 2006) with assimilated altimeter data. Sea surface height (SSH), anomalies (SSHA) and also the sea surface gradient causing the EAC, are prescribed using TOPEX/Poseidon, JASON-1 altimeter data. The lateral open boundary conditions are implemented as radiative conditions according to Flather (1976). A quadratic bottom drag formula at the sea floor is used with a bottom roughness length of $z_0 = 0.002$ m. At the open-ocean boundaries we prescribe profiles of temperature and salinity that are derived from the global ocean model OCCAM (Saunders et al. 1999), which has a horizontal resolution of 1/4 °and 66 vertical z-levels. Because the OCCAM model data set only provides five day averaged fields, the open ocean boundary conditions are therefore updated every fifth day.

3.3 Model design

The model domain is resolved using a coarser grid for the outer area and a finer grid for Hervey Bay (one way nesting). The outer domain (see Fig. 1) is a orthogonal grid of 90×140 points. It covers the region from 151-155 W and 23-28 S. The mesh size varies and increases from 2.5 km within Hervey Bay to 7 km near the boundaries of the model domain. The model bathymetry is extracted from a high resolution bathymetry which provides a horizontal resolution of 250 m. The vertical grid uses 18 sigma levels with a higher resolution towards the sea surface and the bottom boundary. The reason is to resolve accurately the upper mixed layer, but also to catch gravity currents at the sea floor. To minimise artificial geostrophic flows due to internal pressure errors caused by the use of sigma coordinates over bathymetry with steep gradients (Haney 1991, Beckman and Haidvogel 1993) the model bathymetry has been smoothed (Martinho et al. 2006). This reduced the artificial flows to less than 5 cm/s at the shelf edge. The maximum depth within the model domain is limited to 1100 m in order to increase the maximum allowable time step to 12 s and 360 s for the barotropic and baroclinic modes, respectively.

The inner domain (indicated by the red dashed box in Fig. 1) has a uniform grid spacing of 1.5 km and a size of 100×120 grid points. To be consistent with the outer domain the maximum depth was again limited to 1100 m, although, the vertical resolution remains the same. The time steps are then 7 s and 140 s for the barotropic and baroclinic modes, respectively. The vertical profiles of U, V, T, S and SSH of the outer model are interpolated onto the grid of the inner model domain.

To initialise the model a spin-up of two years (1988-1990) was used, starting from rest with climatologically profiles for salinity and temperature. The numerical experiments analysed for this study cover the period 1990-2007.

4 Data

Hydrographic observations, made during three one-week field trips into the bay in September 2004, August and December 2007 (Ribbe 2008b) and Advanced Very High Resolution Radiometer (AVHRR) sea surface temperature (SST) data (three day composites) from 1999-2005 are utilised to validate the performance of the model. The sampling of the September 2004 field trip, sample locations, as well as an analysis of the hydrographical situation within the bay is presented by Ribbe (2006). To be consistent with the 2004 field trip, the sampling locations for the subsequent cruises (August 2007 and December 2007) were the same.

Hourly tidal observations for model validation were taken from seven tide gauges (Fig. 1) for the whole year 2006. The data for Bundaberg and Brisbane were taken from the Joint Archive for Sea Level of the University of Hawaii, which are integrated into the Global Sea Level Observing System (GLOSS). The data for the remaining five gauges were provided by the State of Queensland, Australia. The sea level data were analysed using the least squares method in MATLAB, referred to as the T_TIDE program (Pawlowicz et al., 2002).

The model forcing consists of three hourly observations of atmospheric variables (10 m wind (u,v), 2 m air temperature, relative humidity, cloud cover, air pressure and precipitation) of weather stations located along the east coast, which were linearly interpolated onto the model domain. The river forcing is taken from daily observations of river discharge gauges. Because the salt load of the river is unknown, the salinity of the river discharge is fixed to 2 psu. To avoid numerical instabilities, the daily river discharge was interpolated onto 3 hour intervals and afterwards smoothed with a running mean filter without changing the total integrated discharge.

In Tab. 1 climatologically data for Hervey Bay are presented. To compare the river discharge with the contributions by precipitation, the fresh water inflow by rivers has been converted to a precipitation equivalent (i.e. the thickness of a virtual freshwater layer) over Hervey Bay.

5 Tidal forcing

5.1 Model validation

The barotropic tides (M_2, S_2, N_2, K_1 and O_1) were calculated and compared with observations at 7 tidal gauges (Fig. 1). The tidal range within Hervey Bay can exceed 4 m; therefore one can expect strong mixing dynamics. To get a feeling for the single constituents, they are separated for Bundaberg as; M_2: 0.87m, S_2: 0.30m, K_1: 0.22m, N_2: 0.19m, O_1: 0.12m. These five principal constituents explain nearly 80% of the total variance of the observed tide in Bundaberg. In Fig. 2 a time series of 40 days for Bundaberg is shown. In Tab. 2 the differences in amplitude and phase for all observation stations are listed. One can see that the root mean square error (RMS) for the amplitude does not exceed 3.4 cm and the phase error is not bigger than 7°. In addition Tab. 2 also shows that some computed results are larger than the observations whereas others are smaller, so it can be assumed that no systematic error is present in the simulations. This good numerical reproduction of the tidal signal in Hervey Bay and surroundings gives confidence in the underlying computed velocities field, although no direct velocity measurements are currently available for comparison.

5.2 Tidal mixing

The hydrodynamical model COHERENS allows to compute the bottom friction velocity and therefore an estimate of the thickness of the bottom boundary layer or Ekman layer thickness δ can be given for different flow regimes (Loder and Greenberg, 1986). The Ekman layer thickness is a measure to describe the region that is controlled by friction:

$$\delta = \frac{c\, u_*}{f} \tag{2}$$

where u_* is the bottom friction velocity, f is the Coriolis parameter and c is a constant that can vary between 0.1 and 0.4 . The friction velocity u_* is calculated as $\sqrt{\tau_B/\rho_0}$, the square root of the bottom friction normalised by the water density. Therefore, the distribution pattern of the bottom boundary layer thickness is similar to the bottom friction. Using a low/medium range value of $c = 0.2$, the thickness of the M_2 Ekman layer in Hervey Bay is estimated to be of the order of the water depth.

In Fig. 2c the ratio of the Ekman layer divided by the local depth is shown. One can see that in the southern part of Hervey Bay and also at Breaksea Spit the ratio exceeds values of 1. Therefore the Ekman layer is much thicker than the local depth and hence the whole water column is dominated by friction and turbulent mixing. Thus one can assume that in these regions the water column is well mixed and stratification is suppressed. Only in the central part of the bay and on the north western shelf the mixing ratio is smaller than 0.5 and hence only parts of the water column are occupied by the bottom Ekman layer.

Fig. 2b shows the maximum M_2 induced tidal currents and the tidal ellipses. It is visible that at Breaksea Spit the currents can reach 1.2 m/s. In the central part of the bay these currents vary between 0.5 - 0.7 m/s. Here the tidal ellipses collapse to a straight line and the water is moved only in the north/south direction. Therefore one can assume that the central part of the bay is also well mixed, because the surrounding regions supply already well mixed water into the central part by tidal swash transport. Consequently, tidal mixing, due to the M_2, alone seems sufficient to mix the water column completely in Hervey Bay. Hence only horizontal gradients/fronts are likely to appear. Fig. 2a shows a time series of tidal gauge data at Bundaberg. In the 40 days time series one can see the fortnightly modulation of the tidal signal. Only during 4-5 days around neap tide the tidal amplitude is less than the M_2 component alone. Therefore in this small time window, tidal mixing is significantly reduced and stratification within Hervey Bay can develop.

If one is looking at the M_2 residual induced transport, on can see (Fig. 3b) that this transport is nearly vanishing. In most parts of the bay the residual currents are less than 1 cm/s. Only at Breaksea Spit and in the mouth region of the Great Sandy Strait they can reach values of 10-15 cm/s. The contributions of the other 4 tidal constituents to the residual flow are negligible. The importance of rotation is also vanishing. In most parts of the bay it is far less than 0.1 cycles/day. Only at Breaksea Spit and in the mouth region of the Great Sandy Strait peak values exists of approx. 1 cycles/day. Therefore one can conclude that the tide in Hervey Bay is responsible for the vertical mixing, but transport processes are dominated by wind and baroclinic forcing. This feature of Hervey Bay is quite surprising. Due to the high tidal range much stronger residual currents should be expected. Furthermore, numerical experiments (not shown here) with barotropic conditions and variations in bottom roughness did not change the residual circulation significantly. It must be concluded that weak residual currents are an intrinsic feature of Hervey Bay.

6 Temperature and Salinity

6.1 Model Validation

The simulated temperature and salinity distribution within Hervey Bay is consistent with the observations during all three field surveys (Fig. 4). Because the simulations reveal that the bay is in parts vertically well mixed throughout most of the year, the depth averaged salinity/temperature distribution is considered here for model validation. The model reproduces the salinity gradient with salinity decreasing in all three field trips from the south west coast towards the northern opening of the Bay (Fig. 4). The comparison with the first survey shows that the salinity gradient is less sharp than indicated by the model. But in general the agreement of the model output and the measurements from each of the field trips is quite well. The model confirms that the coastal region is occupied by a zone of hypersalinity with salinities well above 36 psu. The observed temperature distribution is reproduced by the model as well. There are some deviations for the September 2004 field trip. The model seems to overestimate the temperature in the near shore region, but both observations and simulated data show a similar pattern. The distribution of temperature is matched by the model for both subsequent field trips.

For further validation, transects of temperature and salinity at the northern opening of Hervey Bay are shown in Fig. 5. One can see that the coastal hypersalinity zone is somewhat wider than the model indicates, but again the patterns are matched. The model also reproduces the bottom cold water pool for the first two field trips.

In order to further demonstrate the model performance, besides the comparison with snapshot in-situ observations, satellite AVHRR SST data for the period 1999 - 2005 have been used for the model validation. From three day averaged model SST data, mean error and standard deviation for the sampling grid of the AVHRR data have been computed. Fig. 6 demonstrates that the mean error nearly vanishes.

The model tends to slightly underestimate the SST in the northern part of the shelf and also in the eastern part of the bay (This is a numerical artefact because like in most sigma-level ocean models, the most upper T-point is treated as sea surface. Therefore the greater the depth the more the T-point deviates from the true sea surface. Hence the most upper T-point underestimates the true SST), but in general the magnitude of the error is still below 0.1 K for the comparison time of 6 years. The plot of the standard deviation shows that the model catches quite well the variations within the bay (σ=0.6 K). In the direction of the northern shelf also the standard deviation slightly increases (σ=0.8-0.9 K). The strong variation in the mean and standard deviation along the Coast of Fraser Island are believed to be caused by the sampling of the satellite data (i.e. problems with shallow water and land-sea transition).

6.2 Stratification within Hervey Bay

The stratification is expressed in terms of a scalar quantity ϕ (Simpson et al. 1990), which is defined as:

$$\phi = \frac{1}{H}\int_{-H}^{0} (\hat{\rho} - \rho(z))gz\, dz; \quad \text{with} \quad \hat{\rho} = \frac{1}{H}\int_{-H}^{0} \rho(z)\, dz \tag{3}$$

where $\rho(z)$ is the density profile over the water column of depth H. ϕ (units J/m^{-3}) is the work required to bring about complete mixing. Recently, this quantity has been also defined as a potential energy anomaly (PEA) (see e.g. Røed and Albertsen 2007).

ϕ is therefore an expression for the competition of stirring (wind stress, tides, waves and currents) and stratification (heating and buoyancy flux due to precipitation and river discharge). Fig. 7 gives time series of daily averaged wind stress, surface to bottom density/salinity difference and ϕ. Looking at the time series of $\Delta\rho$, one can see that the maximum difference is of the order 0.4 kgm^{-3}. These peak values appear mostly in spring and early summer. Cold "winter" water residues at the bottom of Hervey Bay, whereas increasing solar heatflux increases the temperature of the upper layers and hence establishes the density difference. It is interesting to note that the time series is rather spiky. The time lag between the spikes is nearly an integer multiple of 14 days and clearly shows the spring/neap cycle of the tide. Therefore during spring tide, tidal mixing almost completely removes any stratification and only during neap tide a short term stratification ($<$ 6 days) can be established.

This analysis is focused on daily averages, excluding daily cycles and intertidal effects (tidal straining). During winter there is no stratification visible. The same signal can also be seen in the time series of ϕ. Most of the time it is less than 2 Jm^{-3} and only in spring and summer the required energy to bring about complete mixing can exceed 5 Jm^{-3}. In contradiction the time series of ΔS is nearly flat. Almost during the whole year the surface to bottom salinity difference vanishes and only during some rare events, the difference can reach -0.4 psu. Negative differences are caused by rainfall events. Positive peaks are associated with bottom flow of cold, "fresh" dense water because these peaks mostly occur during late winter. Due to this rather flat time series one can assume that the main contribution to stratification is from thermal effects. A second reason for dominating thermal stratification is the short duration of these events. There is not enough time that saline two layer structures can develop.

An additional source of mixing is energy input due to wind stress (Fig. 7a). One can see that during light wind conditions, stratification can develop (as expected) but that the additional wind energy, during medium/high wind conditions, can completely mix the water column even during neap tide.

6.3 Inverse state and hypersalinity

The hydrographic observations made during the three field surveys indicate that hypersalinity is likely to be a reoccurring climatological feature characterising the bay.

Climatological data for evaporation, precipitation and river runoff (see Tab. 1) show that evaporation with about 2 m/year by far exceeds the supply of freshwater into the bay from precipitation with about 1 m/year and very low river run-off (see Ribbe 2006 for details). The application of the ocean model allows investigating the distribution of salinity throughout time. In fact, the time averaged distribution of salinity in the bay (Fig. 9) and its surroundings confirms that the hypersalinity zone is a climatological feature for the period 1990-2007. The climatological mean value for the salinity gradient in the bay is in the order of about 0.5 psu with salinities near the south west of > 36.1 psu and near the open ocean in the north east of about < 35.5 psu. The magnitude of these gradients correspond to those observed during the three surveys.

To describe the temporal evolution of the hypersalinity zone within Hervey Bay the salinity/density gradient along the indicated transects in Fig. 9 has been computed. Firstly, the focus is on the transect that is placed within Hervey Bay. The transect is aligned perpendicular to the isolines of the climatological salinity distribution. Fig. 8 provides an indication of the temporal evolution of these gradients. They are plotted as psu/km and kg/m^3/km. To quantify these gradients the approach of Largier et al. (1997) is followed in defining hypersalinity and the inverse state of an estuary/bay as: "*... hypersaline is defined as salinities significantly greater than that of the ambient and inverse as densities significantly greater than that of the ambient...* ". By salinities significantly greater, the authors conceive of a salinity S that exceeds the ambient salinity S_0 by more than typical synoptic (i.e. multi-day) fluctuations in the salinity of the ambient. The standard deviation of the ambient salinity over the period of hypersalinity, serves as an appropriate index of the size of these fluctuations. Thus, $(S - S_0) > \sigma$ defines hypersalinity. For the case of Hervey Bay these fluctuations are or the order σ=0.15 psu and in terms of the salinity gradient $\sigma_{Grad} \approx 2\cdot 10^{-3}$ psu/km and therefore one third of the climatological gradient. This implies that Hervey Bay can be classified as a hypersaline bay.

To define the inverse state a dynamical approach is used here. To have a Hervey Bay specific threshold for the inverse state, the density gradients are converted into geostrophically induced velocities, serving as a rough indication. Because tidal mixing is quite high and therefore turbulence is essential in this coastal environment as demonstrated above this indicator should be handled with care.

If one computes the geostrophic residual velocity, caused by a mean density difference of 0.45 kg/m^3 over a distance of 65 km (see Fig. 9), this will result in a flow of approx. 3-5 cm/s. This is in the range of wind induced residual circulations (Fig. 3). Here we assumed a wind speed of 7 m/s, which is the mean climatological average. Hence a geostrophic flow could balance a northerly wind induced circulation. Thus density gradients exceeding 0.01 kgm^{-3}/km can be dynamically important for Hervey Bay.

In Fig. 8bc these critical values are indicated by the red dashed lines. As stated in the description of Hervey Bay, a special feature of it is an aspect ratio of nearly 1, i.e. the width of the connection to the open ocean is equal to the length of the bay itself. For Spencer Gulf, Gulf of California and Ria of Pontevedra this ratio exceeds a value of 3. Therefore Hervey Bay is better described as an "open" coastal environment than to fit into a classical inverse estuary type classification. Further due to its low aspect ratio the bay can not support high salinity/density gradients like for instance Spencer Gulf with peak salinities of > 50 psu in the headwater of the gulf.

To understand if these gradients are Hervey Bay specific or if they reflect simply the variation in the usual subtropical near shore hypersalinity zone (Tomczak and Godfrey 2003), two additional transects (see Fig. 9) have been investigated in the model domain. One is situated at the northern shelf of Hervey Bay and the other is placed approx. 80 km south of Fraser Island.

Tab. 3 shows the comparison of the two additional transects with the gradients in Hervey Bay. The density and salinity gradients are a factor of two higher than the ones computed at the northern shelf. Interesting to note is, that the mean values for the southern transect are nearly vanishing. Secondly if one compares the standard deviation for the three transects, the numbers indicate, that the dynamics within Hervey Bay are much higher than for the surrounding near shore areas. By comparing the correlation of the time series, it is visible that the exchange of water of Hervey Bay and the northern shelf is much higher, than with the region south of Fraser Island.

Concluding from Tab. 3 one can say that the dynamics and magnitude of the gradients in Hervey Bay are higher than in the surrounding coastal waters and therefore these gradients are indeed established by the local dynamics within the bay.

If one looks onto the salinity gradient time series in Fig. 8 one can clearly see a seasonal pattern. The annual cycle is mainly caused by three mechanisms. At first, due to the annual variation in solar heat flux the evaporation rate is triggered by this signal. During summer the evaporation reaches a maximum (see Tab. 1). Because Hervey Bay is in the western part much shallower than in the eastern part, the effective evaporation (E/H - the ratio of evaporation and depth) is at the western shore higher and this leads to a strengthening of the salinity gradient. During winter the whole process is reversed and can weaken or even reverse the gradient. The second mechanism that causes the annual variations is the different residual flow pattern in Hervey Bay. During summer the dominant wind direction is southeast whereas during winter the region is controlled by north easterly trade winds, averaged wind speed are approx. 7 m/s. During SE winds a clockwise circulation exists in the bay (see Fig. 3c). Ocean water of “low” salinity enters the bay via Breaksea spit and leaves Hervey Bay along the western shore. Combined with the higher effective evaporation in the western part, the gradient is strengthened. In contradiction, under NE-wind conditions the whole circulation pattern reverses. Now saline western shore water is pushed into the bay and the salinity gradient is weakened, even if there exist a hypersalinity zone close to the shore. To quantify the impact of both contributions a typical evaporation time scale is computed as:

$$T_{evap} = \frac{H\ \sigma/S_0}{E - P - R} \tag{4}$$

where H denotes the mean depth, σ the size of the salinity fluctuations around S_0 and in the denominator are the contributions of the fresh water balance (evaporation, precipitation and river discharge). This gives an average T_{evap} of 15 days. Ribbe et al. (2008) computed typical water exchange time scales for Hervey Bay as 65 days. Therefore the evaporation water loss dominates the salinity gradient rather than the movement of saline water due to residual circulations.

A third more random mechanism is provided by significant rainfall events accompanied by somewhat delayed higher river discharges, i.e. the salinity near the coast is lower than towards the open ocean. This is for example the case during 1996 when the strongest reversal is observed. Closer inspection of the time series (not shown here) for surface freshwater fluxes due to rainfall and river discharges reveal that during this year a particular wet winter prevents the maintenance of a hypersalinity zone from about April to November 1996. With the approach of summer and an increase of evaporation and no further significant freshwater discharges, the hypersalinity zone reforms (Fig. 8c). The negative peaks in the salinity gradient for January 1992 and January 1999 are caused by massive river discharge of the Mary River. Heavy rainfalls in the catchments area of the river caused these unusual events.

It is interesting to note that during the last decade less frequent reversals of the salinity gradient occurred. This is due to the reduced supply of freshwater to the region as a result of the ongoing drying trend at the central east coast.

To further understand the impact of this drying trend, the days in the year are computed, where the salinity gradient and the density gradient exceed the critical thresholds, as defined above. The results are shown in Fig. 10. A linear fit has been added to both time series. Hervey Bay is on average on 210 days of the year in a hypersaline state and in the inverse state for 95 days, respectively. Interesting to note is that due to the ongoing drying trend, both time series show a rising trend. The model simulations indicate an increase of 2.7 days per year, where Hervey Bay is hypersaline and an increase of 3.8 days per year for inverse conditions. The trends might be judged with care. Especially the annual variation for the inverse state are higher than the linear fit suggest. For inverse conditions the trend is much more visible. One has also to note that we used these measures to show how the reduction of freshwater supply (due to the ongoing drying trend) impacts on the physics of the bay. They are not intended to proof climate change.

6.4 Evaporation induced circulations

Due to the net loss of water (by evaporation) and to maintain the waterbalance within the bay, an inflow of water from the ocean is required. As one can see in Tab. 1 the annual loss of water is approx. 800 mm or 130 m^3/s (Hervey Bay covers approx. 4000 km^2, assuming that the northern boundary of the bay is located at 24.8°S). This would result in a balancing oceanic inflow of 0.1 mm/s. Much more important than this inflow are the effects of the accumulation of salt within Hervey Bay. In the case that Hervey Bay would be an enclosed water body; this water loss would cause an increase of salinity of 2 psu per year (assuming conservation of salt). Because there is no evidence that the salinities are generally increasing in Hervey Bay, a process of salt removal has to be at work.

A simple water and salt balance is considered here. It is assumed that there are two components of salinity induced circulations. The first component (as stated above) is the volume loss due to evaporation. This is a pure inflow, with average velocity u_I.

Thus continuity of volume requires:

$$u_I \; b \; h = A \; (E - P) \tag{5}$$

where E is the evaporation rate, P the precipitation rate, b the width of the opening of Hervey Bay, h the average depth and A the surface area of the bay.

The second component represents all the inflows/outflows, at velocity u_C, which account for the removal/entry of saline water. It is assumed that there exists a circulation that brings shelf water of low salinity into the bay and removes water of higher salinity from Hervey Bay. Therefore salinity continuity requires:

$$\frac{h}{2} u_C \; b \; S_I + u_I \; b \; h \; S_I = \frac{h}{2} u_C \; b \; S_O \tag{6}$$

where u_C is the circulation velocity, S_I the salinity of the water entering the bay and S_O is the salinity of the outflowing water. Using (5) and (6) one obtains:

$$u_C = \frac{2 \; (E - P) \; A}{b \, h} \frac{S_I}{S_O - S_I} \tag{7}$$

This simple model describes how, at a given rate of evaporation, water leaves the bay with higher salinities than the salinities of the inflowing waters. Further one can see that the salinity difference increases as the circulation velocity u_C decreases.

In Fig. 11 a transect through the northern opening of the bay is shown. One can see (Fig. 11a) the average salinity distribution for the whole simulation time (1990-2007). This is used to estimate S_I with 35.5 psu and S_O with 36 psu, further b with 60 km and h with 20 m. $(E-P)$ is estimated with 0.8 m/yr (Tab. 1). This yields a circulation velocity u_C of approx. 0.02 m/s. To compare the performance of this simple analytical model, Fig. 11b shows the average velocity of the north/south component of the flow. All barotropic residuals have been removed here therefore only the evaporation induced velocity fields are visible. One can see, that the peak inflow/outflow velocity is in the range of 3 cm/s and that u_C with 2 cm/s agrees well with the model output. Also visible is that the residual flow shows a tilted left/right separation. Therefore Hervey Bay does not show the typical two layered structure with the inflow of low saline water in the surface layer and the outflow of dense high saline water at the bottom. Thus the bay shows a superposition of a horizontal circulation and a weak two layered structure in the vertical.

This is the result of the strong tidal mixing in and at the northern part of the bay

(Fig. 7c). Because a classical vertical two layer structure cannot be established, the water exchange is realised by an inflow of ocean water in the eastern part of the bay and an outflow at the western shore. If one is looking on the east/west component of the velocity (Fig. 11c) on can see the fingerprint of the inverse circulations. At the western shore there is a weak eastward directed flow close to the bottom. This agrees well with the salinity distribution (upper picture). Here one can see the tilting of the isolines, which indicates an outflow of saline water down the slope. Therefore Hervey Bay shows an inverse circulation pattern with inflow of fresh water at the surface and an outflow of dense/saline water at the bottom.

To quantify the overall residual mass flow, the salinity flux of the bay has been calculated explicitly by computing the transport through advection and diffusion across the open boundaries (Ω) of Hervey Bay. The northern boundary is defined along 24.8°S and the southern boundary is located in the Great Sandy Strait at 25.5°S.

$$F_{Salt}(t) = \int_{\Omega} \left[v(x,z,t)S(x,z,t) \; + \; K_H(x,z,t)\frac{\partial}{\partial y}S(x,z,t) \right] \, d\Omega \tag{8}$$

The first term represents the flux by advection (meridional velocity times salinity) whereas the second term represents the diffusive fluxes. K_H is the turbulent scalar horizontal diffusivity. A rough estimate, to get a feeling for the importance of both contributions to the integral, can be given by estimating the average advective transport with 4 kgm/s, assuming a residual current of 0.1 m/s. The model predicts a bay average turbulent diffusivity of 30 m^2/s. which is used to estimate the diffusive transport. If one estimates the salinity gradient from the climatology (10^{-5} psu/m), this results in an average diffusive transport of approx. $3 \cdot 10^{-4}$ kgm/s. Therefore the advective transport is at least three orders of magnitude larger than the diffusive transport. Integrating, both fluxes explicitly along sigma-coordinates, over the domain, the transport/export of salinity is estimated to be in the order of about 4.0 tons/s (Fig. 8a). If one uses the climatological values (Tab. 1), the net loss of 800 mm would result in an outflow of 3.7 tons/s, which is in good agreement with the numerical results.

The model indicates that since 1990, the salinity flux has increased by about 25 % (linear fit in Fig. 8a, but not shown). Shi et al. (2008a) pointed out, that the total annual mean rainfall in the region has significantly decreased over the last 50 years and the drying has accelerated in particular during the last 20 years. The trend, visible in the forcing time series used in this study, is estimated with a reduction of 5 % in precipitation and 15 % in river discharge. These trends would lead to a rise in the salinity flux to 4.5 ton/s (21% increase during the last two decades) which is again comparable with the model predictions.

Finally the magnitude of these fluxes can be compared with estimates for Spencer Gulf, Australia (Nunes Vaz et al. 1990). Both coastal embayments are comparable in size and atmospheric forcing. The estimated volumetric flux for Spencer Gulf is of the order of 0.05 Sv (Ivanov et al. 2004). If one converts the peak flux (Fig. 8a) into a volume flux, this is estimated to be 0.006 Sv and therefore one order of magnitude smaller. This is not surprising, because Hervey Bay only covers 1/5 of the area of Spencer Gulf. Secondly the aspect ratio (length to width ratio) of Hervey Bay is nearly 1 whereas for Spencer Gulf this is in the range of 3. Hence Hervey Bay is more an open environment than that of a classical gulf shape and can therefore not support high salinity gradients and it is also much more affected by water exchange with the open ocean. If one takes these factors into account (assuming linear scaling, by multiplying the flow of Hervey Bay by an area correction of 5 and an aspect ratio correction of 2-3), the relative volume transport is comparable with Spencer Gulf even if Hervey Bay is smaller in size and constrained by the geometry.

The analysis of the simulations further showed that the annual mean heat content of the bay, solar heat flux and air temperature remain nearly constant over the whole simulation period. They are only responsible for the intra-annual variability. The most important factor influencing the rising trend in the salinity gradient/salinity flux is therefore the positive difference between evaporation and precipitation/river discharge.

7 Conclusion

Climatological data indicate that Hervey Bay is a hypersaline bay that also exhibits features of an inverse estuary, due to the high evaporation rate of approximately 2 m/year, a low precipitation rate of less than 1 m/year and an on average almost absent freshwater input from the two rivers that drain into the bay.

In this study the ocean model COHERENS has been applied to compute the temperature and salinity distribution within the bay. A model validation and calibration has been carried out using recent in-situ field and satellite AVHRR SST data. Observations and model results show that the bay is in parts vertically well mixed throughout the year. The absence of longer lasting stratification is caused by the tidal regime within Hervey Bay. The tidal range can exceed 4 m. Due to the tidally induced bottom shear, most of the time the whole water column is controlled by the bottom Ekman layer. Therefore only horizontal fronts appear. Only during a short time around neap tide, a temperature induced stratification can develop and the bottom to surface density difference can exceed 0.3 kg/m^3. The dominant mechanism forcing residual circulations in the bay is provided by the Trade winds from the east with a northern component in autumn and winter and a southern one in spring and summer. These wind-induced currents are in the range of 5-10 cm/s. The contribution of the tides to the residual currents is negligible. Hence the tide is only responsible for mixing.

As in other inverse estuaries, the annual mean salinity increases towards the shore to form a nearly persistent salinity gradient. The region therefore acts as an effective source of salt accumulation and injection into the open ocean. The high evaporation is leading to a loss of freshwater and increases salinity within the bay. The average salinity flux into the open ocean is estimated to be about 4.0 tons/s. This study showed that this transport is mainly caused by advective transport, whereas the diffusive transport is on average three orders in magnitude smaller.

Further the evaporation loss and the accumulation of salt within the bay leads to an evaporation induced residual circulation of the order of 2-4 cm/s. The simulations demonstrated that the salinity flux increased by 25% in the last two decades. This is due to an ongoing drying trend at the East Coast of Australia. The climate of subtropical eastern Australia has changed during the last few decades, and this study indicates that hypersalinity conditions are more persistent. The number of days, during which Hervey Bay is dominated by hypersalinity, is on average 210 but shows a rising trend with an increase of 3 days per year. Also the time duration of inverse conditions is increasing.

During the study period, salinity fluxes have increased, and the reversal of hypersalinity conditions are less frequent in the last decade due to the reduced supply of freshwater. This study clearly demonstrates that recent climate trends impacted on physical marine conditions in subtropical regions of eastern Australia and are likely to do so in the future if current climate trends (drying) are to continue.

Acknowledgements We would like to acknowledge financial support for this study provided by the Burnett Mary Regional Group, Australia, the Hanse Institute for Advanced Study, Delmenhorst, Germany and the Universitäts-Gesellschaft Oldenburg (UGO). We also gratefully acknowledge the Bureau of Meteorology, Australia, Geoscience Australia and CSIRO Marine and Atmospheric Research for providing various data for this study.

References

39. Beckman A, Haidvogel D (1993) Numerical simulation of flow around a tall isolated seamount. J Phys Oceanography 23:17361753

39. Beer T, Borgas M, Bouma W, Fraser P, Holper P, Torok S (2006) Atmosphere. Theme commentary prepared for the 2006 Australia State of the Environment Committee, Department of Environment and Heritage, Canberra

39. Bignami F, Marullo S, Santoleri R, Schiano ME (1995) Longwave radiation budget in the Mediterranean Sea. J Geophys Res 100(C2):2501-2514

39. Brink KH, Shearman RK (2006) Bottom boundary layer flow and salt injection from the continental shelf to slope. J Geophys Res Lett 33:L13608

39. Cai W, Shi G, Cowan T, Bi D, Ribbe J (2005) The response of the southern annual mode, the East Australian Current, and the southern mid-latitude ocean circulation to global warming. J Geophys Res Lett 32:L23706

39. deCastro M, Gomez-Gesteira M, Alvarez I, Prego R (2004) Negative estuarine circulation in the Ria of Pontevedra (NW Spain). Est Coast Shelf Sci 60:301-312

39. Fairall CW, Bradley EF, Rogers DP, Edson JB, Young GS (1996), Bulk parametrisation of air-sea fluxes for tropical ocean-global atmosphere Coupled-Ocean Atmosphere Response Experiment. J Geophys Res 101:3747-3764

39. Fairall CW, Bradley EF, Hare JE, Grachev AA , Edson JB (2003) Bulk Parameterization of AirSea Fluxes: Updates and Verification for the COARE Algorithm. J of Climate 16:571-591

39. Flather RA (1976) A tidal model of the northwest European continental shelf. Memories de la Societe Royale des Sciences de Liege 6 10:141164

39. Geernaert GL, Katsaros KB, and Richter K (1986), Variation of the drag coefficient and its dependence on sea state. J Geophys Res 91:7667-7679

39. Haney RL (1991) On the Pressure Gradient Force over Steep Topography in Sigma Coordinate Ocean Models. J Phys Ocean 21:610-619

39. Ivanov VV, Shapiro GI, Huthnance JM, Aleynik DL, Golovin PN (2004) Cascades of dense water around the world ocean. Prog in Ocean 60:47-98

39. Josey SA, Pascal RW, Taylor PK, Yelland MJ (2003) A New Formula For Determining the Atmospheric Longwave Flux at the Ocean Surface at Mid-High Latitudes. J Geophys Res 108(C4)

39. Largier JL, Hollibaugh JT, Smith SV (1997) Seasonally hypersaline estuaries in Mediterranean-climate regions. Est Coast Shelf Sci 45:789-797

39. Lavin MR, Godinez VM, Alvarez LG (1998) Inverse-estuarine Features of the Upper Gulf of California. Est Coast Shelf Sci 47:769-795

39. Loder JW, Greenberg DA (1986) Predicted positions of tidal fronts in the Gulf of Maine region. Cont Shelf Res 6:394414

39. Luyten P J, Jones JE, Proctor R, Tabor A, Tett P, Wild-Allen K (1999) COHERENS - A coupled hydrodynamical-ecological model for regional and shelf seas: user documentation, MUMM Rep., Management Unit of the Mathematical Models of the North Sea

39. Lyard F, Lefevre F, Letellier T, Francis O (2006) Modelling the global ocean tides: modern insights from FES2004. Ocean Dynamics 56:394-415

39. Martinho AS, Batteen ML (2006) On reducing the slope parameter in terrain-following numerical ocean models Ocean Modelling 13:166175

39. Mellor GL, Yamada T (1982) Development of a turbulence closure model for geophysical fluid problems. Rev Geophys Space Phys 20:851-875

39. Middelton JH, Coutis P, Griffin DA, Macks A, McTaggart A, Merrield MA, Nippard GJ (1994) Circulation and Water Mass Characteristics of the Southern Great Barrier Reef. Aust J Mar Freshw Res 45:1-18

39. Monin A, Obukhov A (1954) Basic turbulent mixing laws in the atmospheric near-surface layer. Trans Geophys Inst Akad Nauk USSR, 151:163187

39. Murphy BF, Ribbe J (2004) Variability of southeast Queensland rainfall and its predictors. Int J Climatology 24(6):703-721

39. Nunes Vaz RA, Lennon GW, Bowers DG (1990) Physical behaviour of a large, negative or inverse estuary. Cont Shelf Res 10:277-304

39. Pawlowicz R, Beardsley B, Lentz S (2002) Classical tidal harmonic analysis including error estimates in MATLAB using T_TIDE. Comput Geosci 28:929937

39. Ribbe J (2006) A study into the export of saline water from Hervey Bay, Australia. Est Coast Shelf Sci 66:550-558

39. Ribbe J, Wolff J-O, Staneva J, Gräwe U (2008a) Assessing Water Renewal Time Scales for Marine Environments from Three-Dimensional Modelling: A Case Study for Hervey Bay, Australia. Env Modelling Software 23:1217-1228

39. Ribbe J (2008b) Monitoring and Assessing Salinity and Temperature Variations in Hervey Bay. Final Report prepared for the Burnett Mary Regional Group, Bundaberg, Australia

39. Roe PL (1985) Some contributions to the modelling of discontinuous flows. In: Proceedings of 1983 AMS-SIAM summer seminar on large scale computing in fluid mechanics, Philadelphia. Lectures in Applied Mathematics 22:163193

39. Røed LP, Albertsen J (2007) The impact of freshwater discharge on the ocean circulation on the Skagerrak/northern North Sea area Part I: model validation. Ocean Dynamics 57:296-285

39. Saunders P, Coward AC, de Cuevas BA (1999) Circulation of the Pacific Ocean seen in a global ocean model: Ocean Circulation and Climate Advanced Modelling project (OCCAM). J Geophys Res 104:18281-18299

39. Seidel DJ, Fu Q, Randel WJ, Reichler TJ (2008) Widening of the tropical belt in a changing climate. Nature Geoscience 1:21-24

39. Shi G, Cai W, Cowan T, Ribbe J, Rotstayn L, Dix M (2008a) Variability and trend of the northwest Western Australia Rainfall: observations and coupled climate modelling. J of Climate 21:2938-2959

39. Shi G, Ribbe J, Cai W, Cowan T (2008b) Interpretation of Australian summer and winter rainfall projections. J Geophys Res Lett 35:L02702

39. Simpson JH, Brown J, Matthews J, Allen G (1990) Tidal straining, density currents and stirring in the control of estuarine stratification. Estuaries and Coasts 13:123-132

39. Smagorinsky J (1963) General circulation experiments with the primitive equations I. The basic experiment. Monthly Weather Review 91:99165

37. Tomczak M, Godfrey S (2003) Regional Oceanography: an Introduction. 2nd edition. Daya Publishing House Delhi, 390 pp

39. Vethamony P, Babu MT, Ramanamurty MV, Saran AK, Joseph A, Sudheesh K, Padgaonkar RS, Jayakumar S (2007) Thermohaline structure of an inverse estuary - The Gulf of Kachchh: Measurements and model simulations. Marine Pollution Bul-

letin 54:697-707

39. Wolanski E (1986) An evaporation-driven salinity maximum zone in Australian tropical estuaries. Est Coast Shelf Sci 22:415-424

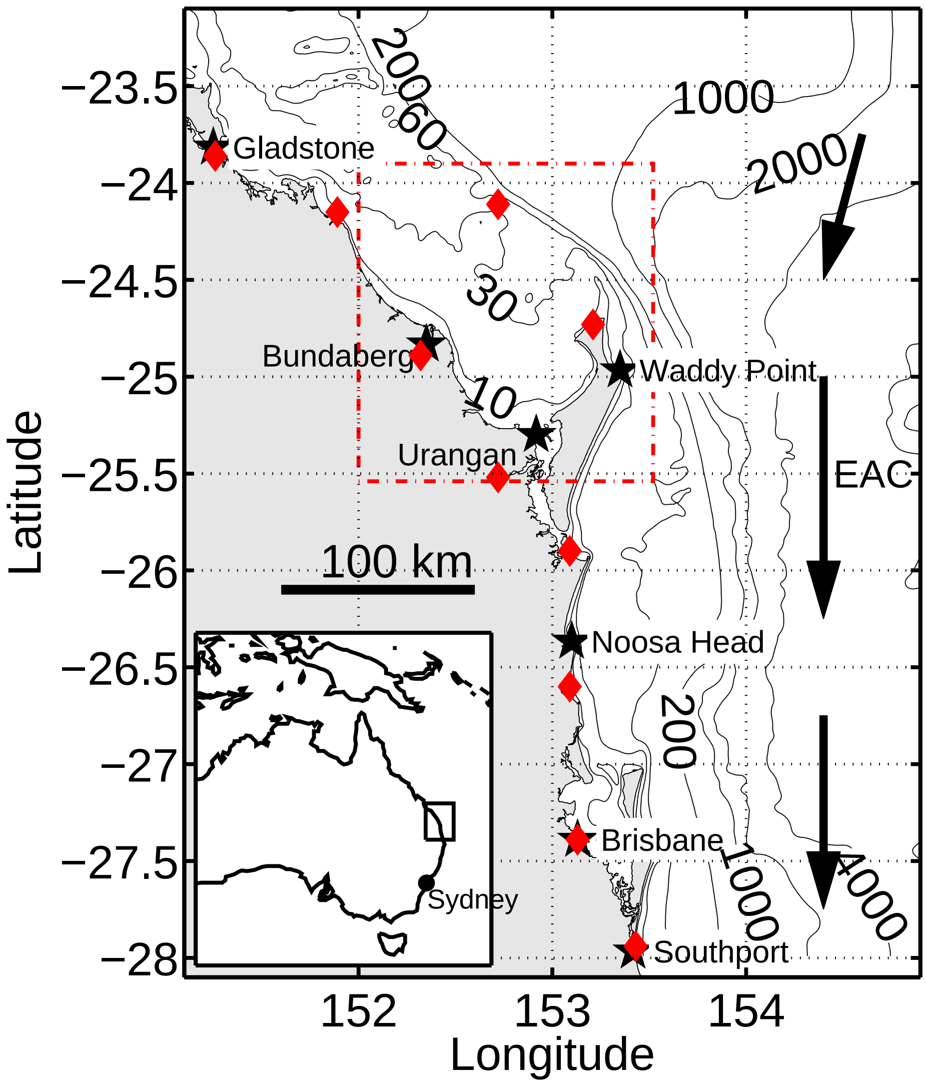

Fig. 1 Model domain and location of Hervey Bay. The isolines indicates the depth below mean sea level. The red dashed box marks the region of interest and also the location of the inner nested model area. The East Australian Current (EAC) is schematically indicated by the arrows. Also plotted are the positions of the tide gauges (black stars). The location of the weather observation stations are shown by the red diamonds. Insert: a map of Australia showing the location of the model domain along the east Australian coast.

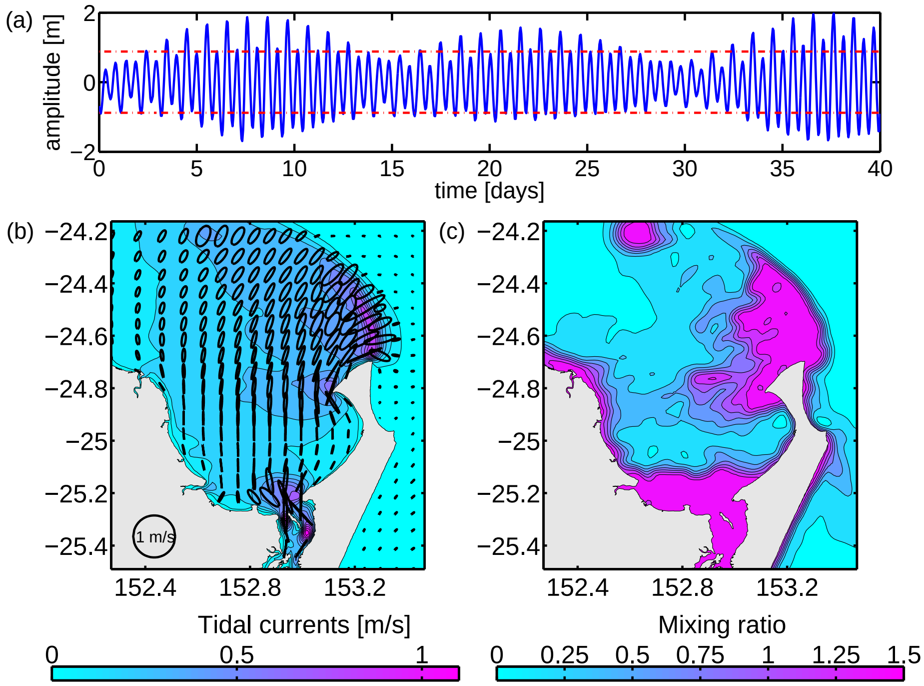

Fig. 2 (a) Arbitrary tidal time series for Bundaberg. Indicated by the red dashed line is the amplitude of the M_2 component, (b) maximum tidal currents (M_2) and also plot of the tidal ellipse and (c) the ratio Ekman layer/local depth. For visualisation purposes this ratio is limited to 1.5. The averaging is done over 5 tidal cycles.

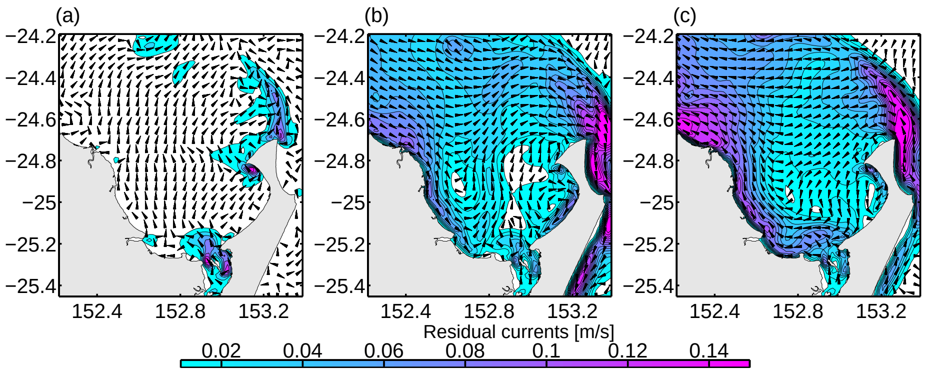

Fig. 3 (a) Depth averaged residual circulations and currents (in m/s) for M_2, (b) idealised NE wind (7 m/s) and (c) idealised SE wind (7 m/s). The magnitude is indicated by the colour code, whereas the arrows are normalised to indicate the direction of the flow. Residual currents below 1 cm/s are marked white. The averaging is done over 5 tidal cycles. The residual currents for the wind forcing are detided.

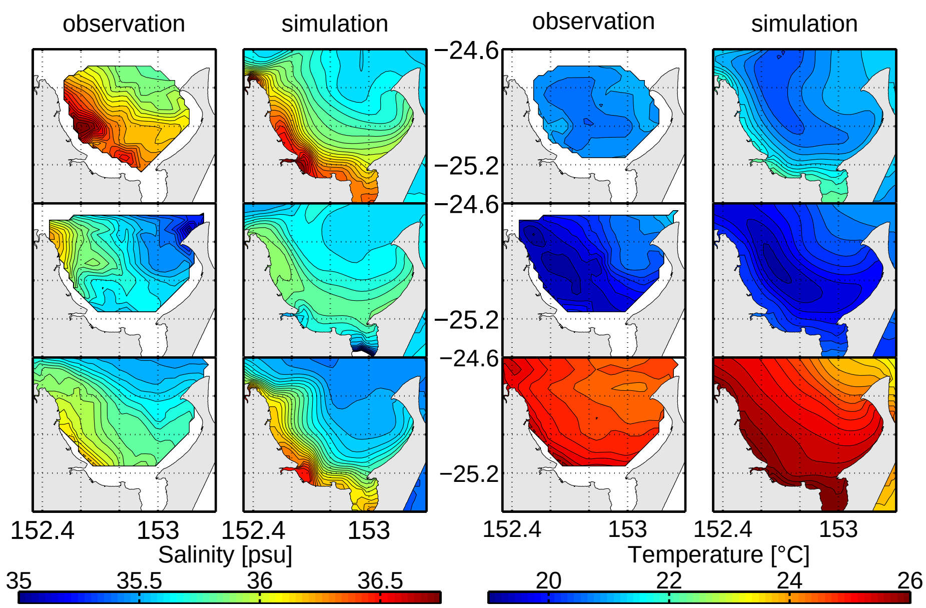

Fig. 4 Comparison of the depth-averaged salinity and temperature distributions during September 2004 (top row), August 2007 (middle row) and December 2007 (bottom row).

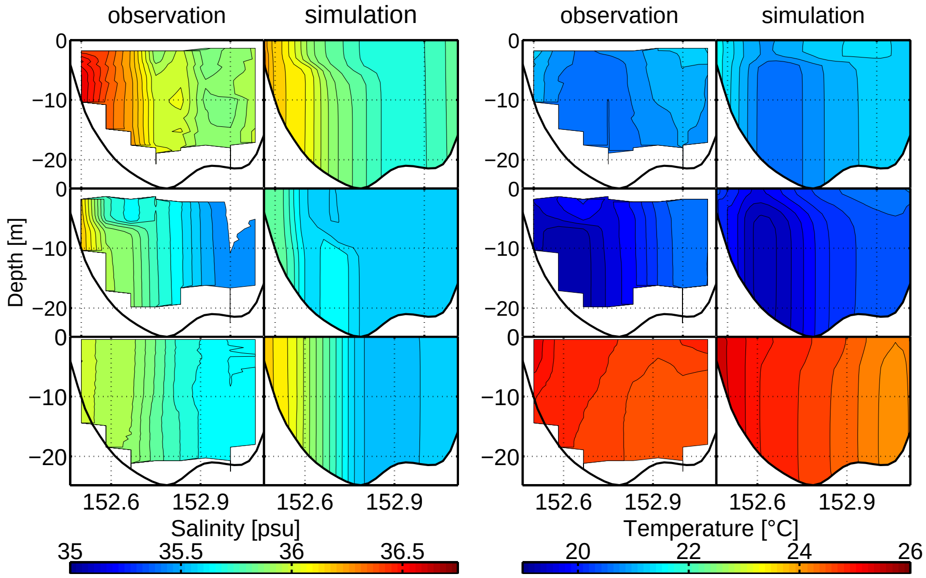

Fig. 5 Comparison of the salinity and temperature transects along 24.8°S latitude during September 2004 (top row), August 2007 (middle row) and December 2007 (bottom row).

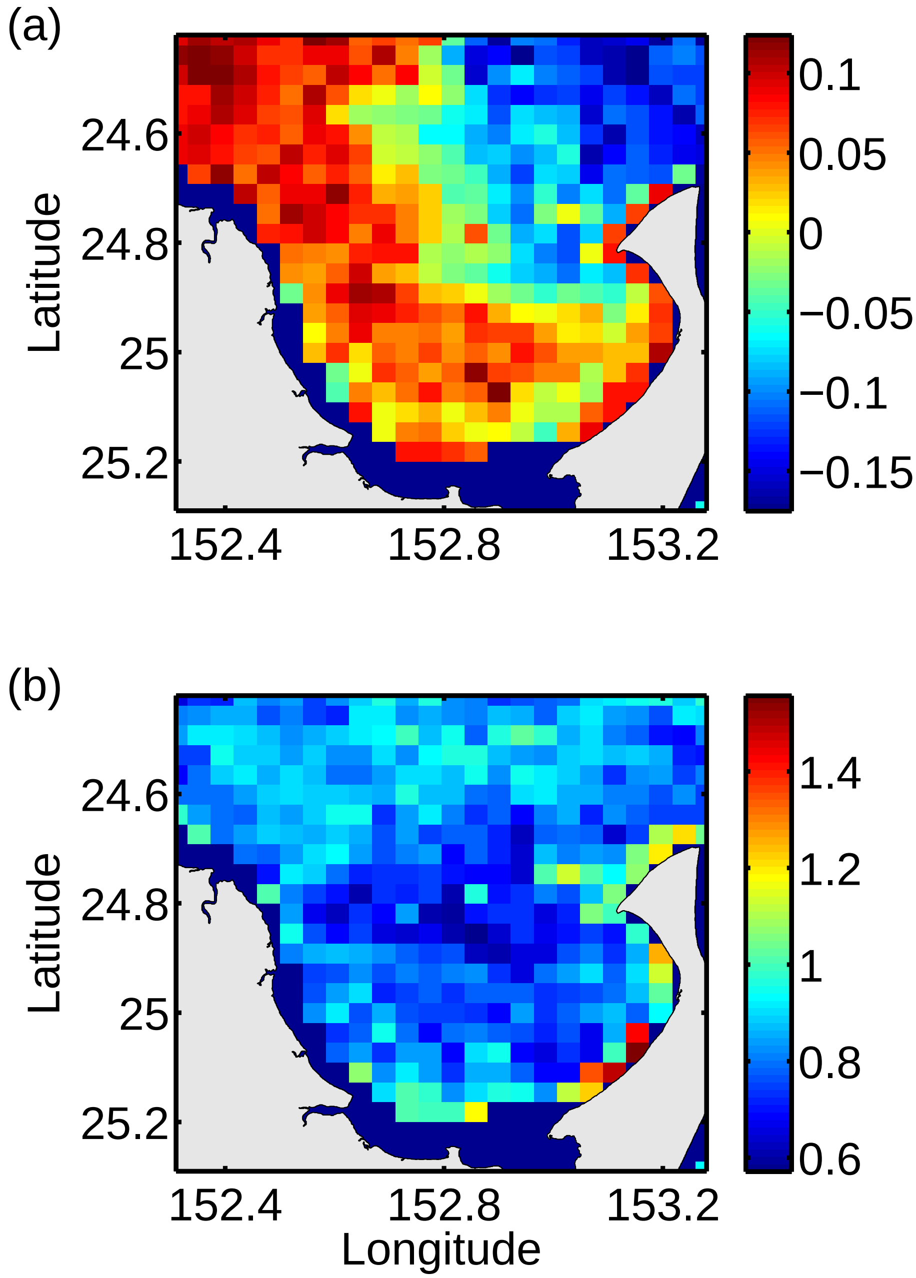

Fig. 6 (a) Mean error - mean(SST$_{Model}$ - SST$_{AVHRR}$) for the sampling grid of the AVHRR satellite data (time span 1999-2005) in Kelvin and (b) standard deviation also in Kelvin.

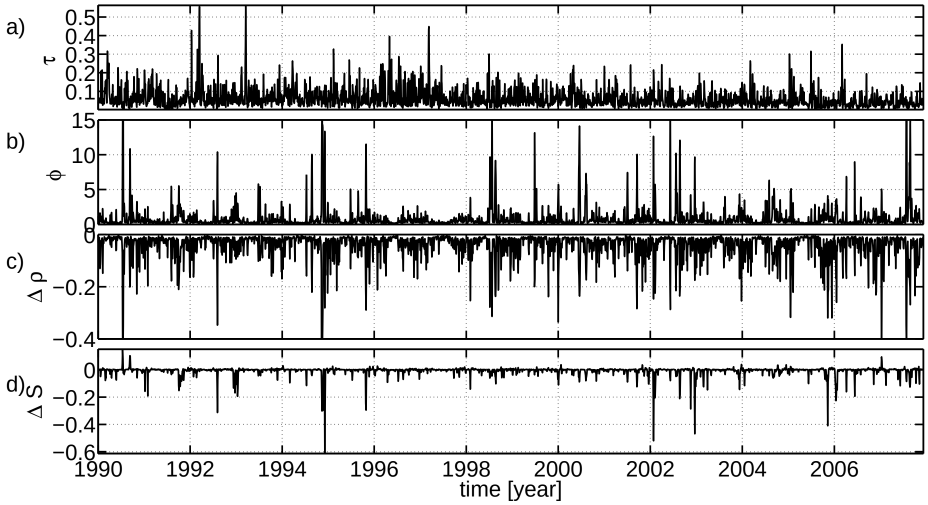

Fig. 7 (a) Time series of wind stress - τ $[Pa]$, (b) stratification index - ϕ $[Jm^{-3}]$, (c) difference between surface and bottom density - $\Delta\rho$ $[kgm^{-3}]$ and (d) difference between surface and bottom salinity - ΔS $[psu]$. Time series for (b), (c) and (d) are only computed in the bay where the depth is greater than 15 m. Shown are daily averaged values.

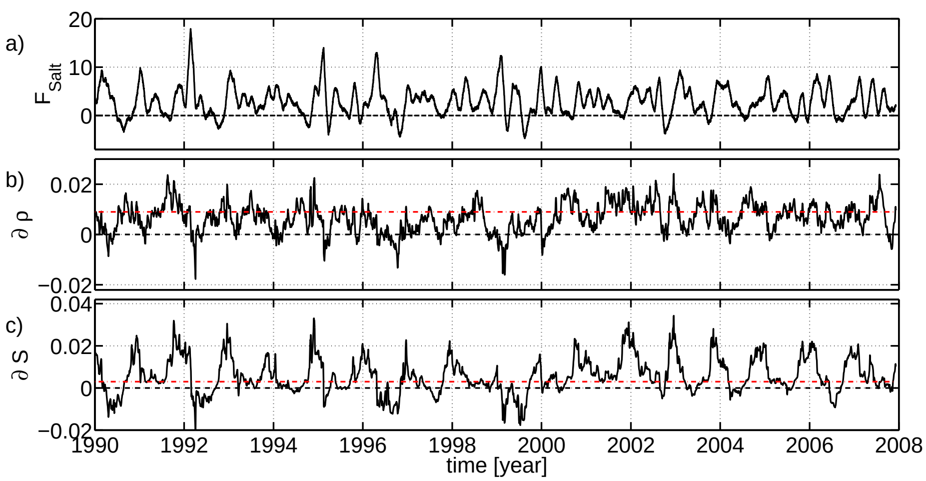

Fig. 8 (a) Time series of salinity flux - F_{Salt} $[ton/s]$, (b) density gradient - $\partial\rho$ $[kg/m^3/km]$ and (c) salinity gradient - ∂S $[psu/km]$ (c). Shown are daily averages. The red dashed lines indicate the thresholds given in the text.

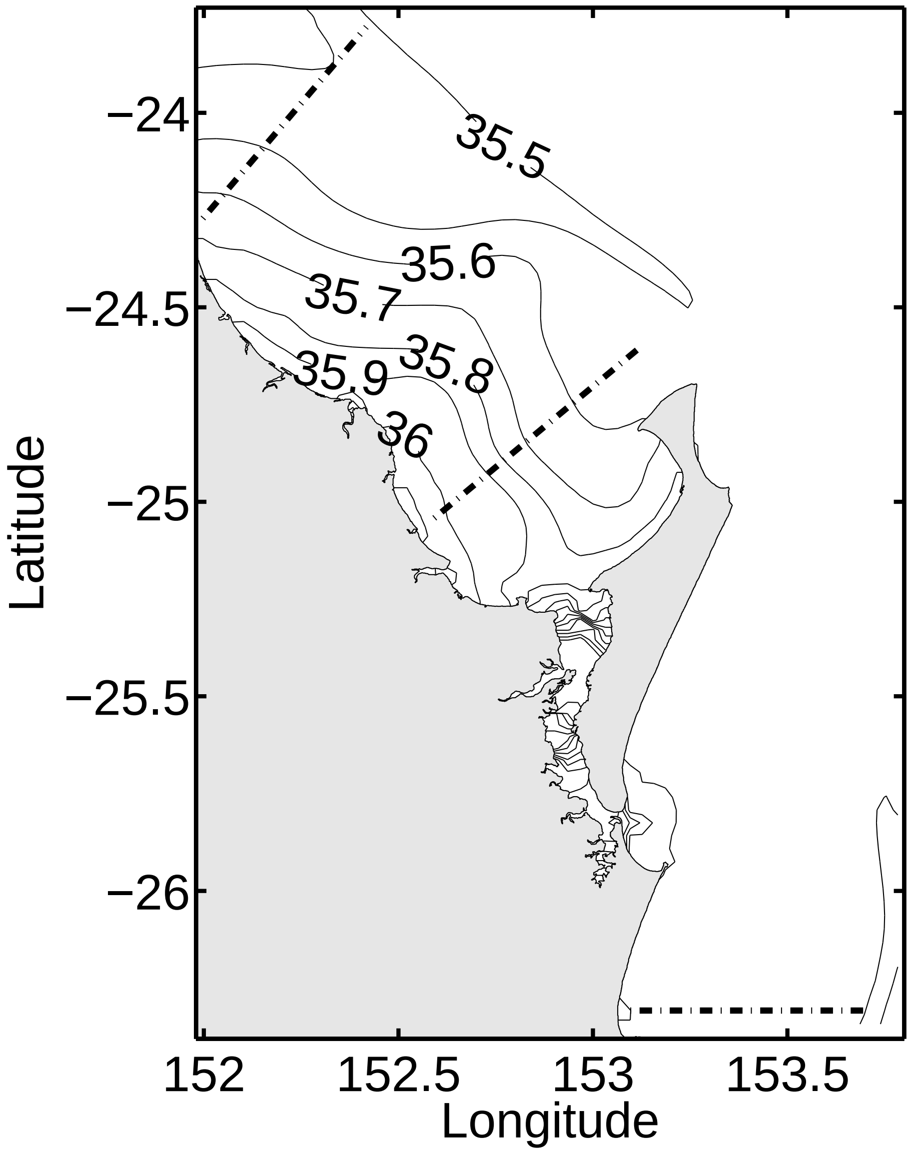

Fig. 9 Mean salinity distribution averaged over the period 1990-2007. Also shown is the position of the three transects to compute the density and salinity gradients.

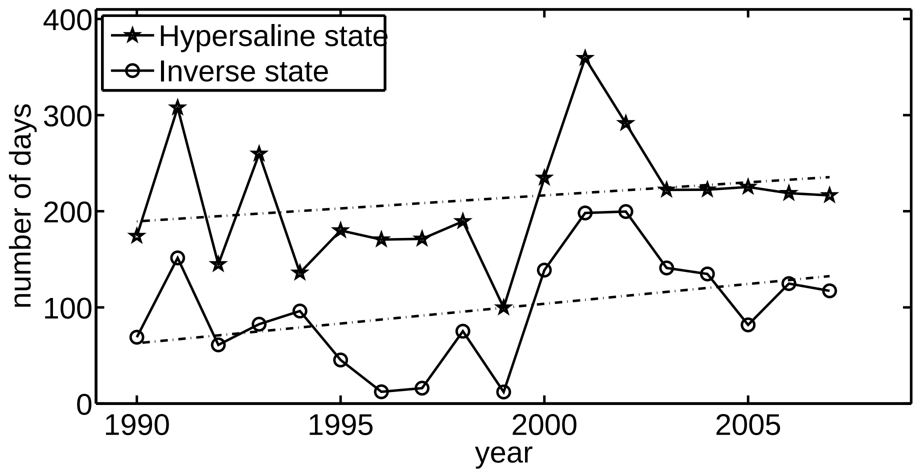

Fig. 10 Number of days in the year where ∂S and $\partial \rho$ exceed the critical thresholds. The two dashed lines are linear fits to indicate the trend.

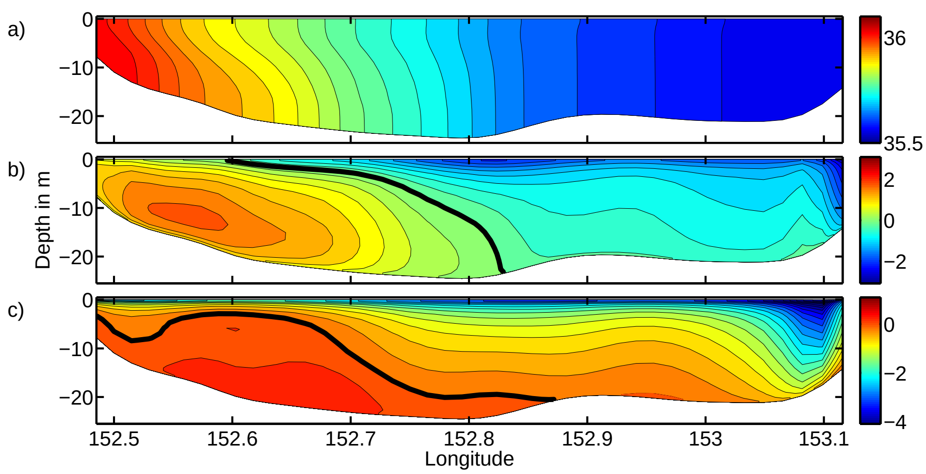

Fig. 11 (a) Average vertical salinity distribution at the northern opening of Hervey Bay in psu, (b) average north/south velocity distribution in cm/s. Positive values indicate a northward directed flow (out of the bay) and (c) average east/west velocity distribution in cm/s. Positive values indicate a eastward directed flow (directed to Fraser Island). The thick black line indicates the change in sign of the velocity components. The transect is placed along 24.8°S latitude. The data are averaged for the whole simulation period (1990-2007).

Table 1 Climatological data of Hervey Bay (southern hemisphere seasons).

	Summer	Fall	Winter	Spring	Annual
Evaporation [mm]	644	455	326	555	1980
Precipitation [mm]	452	230	126	200	1008
River discharge [mm]	72	66	25	11	174
Wind speed [m/s]	6.4	6.2	5.6	6.6	6.2
Wind direction [degree]	86	120	170	48	107
Air temperature [°C]	25.1	22.2	16.8	21.9	21.5

Table 2 Comparison of observed and modelled tidal elevation and phase at reference sites forced by five tidal constituent. The deviations are computed as Δ=observation-simulation. The tidal amplitude error $\Delta\zeta$ is given in cm and the phase error $\Delta\psi$ in degree.

	M_2		S_2		K_1		N_2		O_1	
Station	$\Delta\zeta$	$\Delta\psi$	$\Delta\zeta$	$\Delta\psi$	$\Delta\zeta$	$\Delta\psi$	$\Delta\zeta$	$\Delta\psi$	$\Delta\zeta$	$\Delta\psi$
Gladstone	4.0	-3.2	-3.0	4.6	2.1	-7.5	1.8	5.5	-3.2	7.7
Bundaberg	3.2	-4.7	2.7	-2.2	-0.9	-10.7	-1.9	-3.2	-0.2	10.1
Urangan	3.5	-4.7	1.8	2.8	-0.4	-5.7	0.9	9.3	-0.5	8.4
Waddy Point	-1.3	0.8	-2.0	-5.6	-0.1	-2.6	-1.3	-3.4	-0.1	-5.9
Noosa Head	-2.8	-6.1	-2.1	-3.9	-1.4	1.9	0.1	-5.4	-1.2	3.2
Brisbane	5.7	-1.2	1.7	7.5	1.4	8.9	2.4	11.7	1.1	6.0
Southport	1.2	0.8	-2.0	-5.6	-0.1	-2.7	-1.0	5.6	-1.1	3.9
RMS	3.4	3.8	2.3	5.8	1.1	6.6	1.5	7.0	1.4	6.9

Table 3 Mean and standard deviation of the salinity and density gradients along the transects indicated in Fig. 9. Also the correlation of the time series for Hervey Bay with the two additional transects time series are given.

	North	Bay	South
$\partial\rho$			
Correlation	0.63	1	0.4
Mean [kgm^{-3}/km]	0.0027	0.0059	0.0004
Std [kgm^{-3}/km]	0.0039	0.0054	0.0028
∂S			
Correlation	0.67	1	0.39
Mean [psu/km]	0.0024	0.0059	0.0002
Std [psu/km]	0.0042	0.0069	0.0012